TRANSIENT RESPONSE OF MAGNETOHYDRODYNAMIC TURBULENCE IN INCOMPRESSIBLE CHANNEL FLOW TO SUDDEN APPLICATION AND REMOVAL OF MAGNETIC FIELD

Kia Makouei and Myoungkyu Lee
Department of Mechanical and Aerospace Engineering
University of Houston
Houston, Texas 77204, United States of America
kabdolla@cougarnet.uh.edu and leemk@uh.edu

ABSTRACT

The transient and spectral response of magnetohydrodynamic wall turbulence to the sudden application and removal of a wall-normal magnetic field is examined through direct numerical simulation of an incompressible channel flow at $Re_\tau = 182$ and $Ha = 6$. The friction velocity overshoots its asymptotic MHD value on switch-on and undershoots the hydrodynamic baseline on switch-off, an asymmetry traced to the separation between the Joule and viscous timescales, and the new steady state carries a wall-shear stress below the hydrodynamic value. The two-point spectral budget of $\langle u'u' \rangle$ reveals that the Lorentz force selectively attenuates the diagonal $k_x^\# \approx k_z^\#$ branch of the production and turbulent transport, and that the magnetic potential term M_{11}^p and the MHD dissipation term M_{11}^d cancel almost exactly over most of the spectral plane, leaving a residual net sink concentrated in the low-$k_x^\#$ range that accounts for the small integrated magnetic contribution previously reported for the streamwise Reynolds-stress budget.

INTRODUCTION

Magnetohydrodynamic (MHD) turbulence in wall-bounded flows of electrically conducting fluids underpins a broad range of technological applications, the most demanding of which is the liquid-metal blanket of magnetic-confinement fusion reactors, in which lead-lithium alloys simultaneously breed tritium and remove the volumetric heat deposited in the breeding zone against the strong toroidal field of the device (Abdou *et al.*, 2015; Smolentsev, 2021; Mistrangelo *et al.*, 2021). Related applications include electromagnetic pumps, metallurgical processing and MHD flow-control devices (Al-Habahbeh *et al.*, 2016; Davidson, 2017). The interaction of the induced current with the imposed field generates a Lorentz force that opposes the fluctuating motion and reshapes the near-wall dynamics, as is now well established for canonical channel and duct geometries (Lee & Choi, 2001; Boeck *et al.*, 2007; Krasnov *et al.*, 2008*a*, 2012; Satake *et al.*, 2006; Yamamoto & Kunugi, 2016; Zikanov *et al.*, 2014). As the Hartmann number is raised, the flow becomes progressively more anisotropic and eventually re-laminarizes once the Lorentz force dominates the inertial dynamics (Zikanov & Thess, 1998; Pothérat & Kornet, 2015; Lee, 2024). Because practical MHD systems routinely operate under time-varying electromagnetic loading during startup, plasma disruptions and shutdown, the temporal response of the turbulence to the sudden application and removal of an imposed field bears directly on their design and control (Yamamoto & Kunugi, 2016; Jiang & Smolentsev, 2024).

Despite this engineering relevance, the quantitative understanding of MHD wall turbulence remains largely restricted to one-point statistics. The steady-state response has been characterized through mean profiles, Reynolds stresses and one-point Reynolds-stress budgets (Lee & Choi, 2001; Satake *et al.*, 2006; Boeck *et al.*, 2007; Krasnov *et al.*, 2008*a*; Yamamoto & Kunugi, 2016; Lee, 2024), following the methodology of Mansour *et al.* (1988) and Lee & Moser (2019). Our previous contribution (Lee, 2024) surveyed wall-normal budget profiles of $\langle u'^2 \rangle$ across a range of Hartmann and Reynolds numbers and identified a reduction of the turbulent production as the dominant suppression mechanism, while the integrated magnetic contribution was found to be comparatively small, in agreement with Yamamoto & Kunugi (2016). Two questions are not addressed by such an integrated view. First, the response of the wall friction and the bulk velocity to a sudden change in the imposed field is intrinsically non-stationary and cannot be inferred from steady-state statistics. Second, the integrated budget conceals the spectral structure of the budget terms and cannot resolve which scales are affected by the Lorentz force. The latter question is naturally posed within the spectral budget framework of Lee & Moser (2019), itself rooted in earlier work on the scale-by-scale energy budget of canonical wall turbulence (De Angelis *et al.*, 2002; Cimarelli *et al.*, 2016; Mizuno, 2016; Cho *et al.*, 2018; Kawata & Alfredsson, 2018). Whether the Lorentz force disrupts the corresponding energy pathway uniformly in scale or acts selectively on particular regions of the spectral plane has received little quantitative attention, in spite of the long-standing observation that the imposed field elongates the near-wall streaks (Lee & Choi, 2001; Boeck *et al.*, 2007; Krasnov *et al.*, 2008*a*).

In this work, both questions are addressed through direct numerical simulation of a turbulent channel flow at $Re_\tau = 182$ subjected to the sudden application and subsequent removal of a wall-normal magnetic field corresponding to $Ha = 6$. The temporal response of the friction velocity and the centerline velocity is tracked through the suppression and recovery transients, and the two statistically steady states bracketing the suppression transient are characterized through the two-point correlation budget of $\langle u'\tilde{u}' \rangle$. The spectral structure of the production and the turbulent transport is examined (Lee & Moser, 2019; Cho *et al.*, 2018; Kawata & Alfredsson, 2018), and the magnetic contribution is decomposed into a magnetic potential term M_{11}^p and an MHD dissipation term M_{11}^d. Three observations organize the analysis. First, the friction velocity overshoots its eventual MHD steady-state value on switch-on and undershoots the hydrodynamic baseline on switch-off, and the new MHD steady state has a wall-shear stress that lies below the hydrodynamic value. Skin-friction reduction by an imposed magnetic field has been documented for spanwise-aligned configurations (Krasnov *et al.*, 2008*b*), but the wall-normal-field case at moderate Ha has, to the authors' knowledge, not been reported to deviate in this direction from the conventional expectation of an enhanced wall-shear stress (Boeck *et al.*, 2007; Krasnov *et al.*, 2008*a*; Lee, 2024). The reduction is in the viscous wall stress alone and does not imply an energy saving, since the integrated Lorentz body force enters the streamwise momentum balance. Second, the two-point spectral budget reveals that the Lorentz force selectively attenuates the diagonal $k_x^\# \approx k_z^\#$ branch of the production and the turbulent transport, so that the surviving turbulent kinetic energy is confined to elongated, streamwise-coherent scales, providing the spectral-budget counterpart of the streak elongation reported in Lee & Choi (2001); Boeck *et al.* (2007); Krasnov *et al.* (2008*a*). Third, the spectral decomposition of the magnetic term shows that M_{11}^p and M_{11}^d are individually large and co-located at $k_x^\# \to 0$, and their near-cancellation in physical space accounts for the small net magnetic contribution previously reported in the integrated budget (Yamamoto & Kunugi, 2016; Lee, 2024), identifying the spectral exchange that allows the streamwise streaks to survive at moderate Ha.

METHOD

Direct numerical simulations (DNS) of incompressible turbulent channel flow are performed in the presence of an imposed uniform magnetic field. The induced magnetic field is negligible compared with the imposed one for most engineering flows of electrically conducting fluids, and the quasi-static approximation valid at low magnetic Reynolds number is therefore adopted throughout (Davidson, 2017). The governing equations for the velocity field $\mathbf{u}$ under a constant magnetic field $\mathbf{B}$ read (Zikanov & Thess, 1998; Lee & Choi, 2001; Satake *et al.*, 2006; Boeck *et al.*, 2007),

$$\nabla \cdot \mathbf{u} = 0 \tag{1}$$

$$\partial_t \mathbf{u} = -(\mathbf{u}\cdot\nabla)\mathbf{u} - \nabla p + \frac{Ha^2}{Re}(\mathbf{J}\times\mathbf{B}) + \nu\nabla^2\mathbf{u} \tag{2}$$

where $\mathbf{J}$ is the current density. The equations are non-dimensionalized using the channel half-width, the bulk velocity and unit density, so that $Re = 1/\nu$ with ν the kinematic viscosity. The Hartmann number is defined as $Ha = 2|\mathbf{B}|\sqrt{\sigma/\nu}$, with σ the electrical conductivity, and the Stuart (interaction) number is $\mathscr{N} = Ha^2/Re$. In the MHD cases reported here the magnetic field magnitude is taken as unity. The current density follows from Ohm's law for a moving conductor together with the constraint of charge conservation, $\mathbf{J} = -\nabla\phi + (\mathbf{u}\times\mathbf{B})$ and $\nabla^2\phi = \mathbf{B}\cdot(\nabla\times\mathbf{u}) = \mathbf{B}\cdot\omega$, where ϕ is the electric potential and ω is the vorticity. A velocity–vorticity formulation is adopted, following standard practice in channel-flow DNS (Kim *et al.*, 1987). The simulations are performed with our in-house code, validated for high-Reynolds-number wall turbulence at $Re_\tau \approx 5200$ (Lee & Moser, 2015) and extended to MHD (Lee, 2024). The simulations are initialized from fully developed turbulent channel flow at $Re_\tau = 182$ in a domain of size $L_x \times L_y \times L_z = 4\pi\delta \times 2\delta \times 2\pi\delta$, where δ is the channel half-width. A wall-normal magnetic field at $Ha = 6$ is then imposed and the response is followed until a new statistically steady state is reached. Once sufficient statistics have been accumulated, the field is removed and the recovery of the turbulence is monitored. All cases are forced at constant mass flow rate, and convergence is verified through closure of the total shear-stress balance, with a residual below 0.1%. All quantities in wall units, including y^+ and the rescaled wavenumbers $k_x^\#$ and $k_z^\#$, are non-dimensionalized using the friction velocity and viscous length scale of the hydrodynamic reference state, following Lee (2024).

The spectral structure of the Reynolds-stress budget is examined through the evolution equation of the two-point correlation tensor $R_{ij} = \langle u_i' \tilde{u}_j' \rangle$, derived from the Navier–Stokes equations augmented by the Lorentz force in a manner analogous to the non-MHD derivation of Lee & Moser (2019) and the classical Reynolds-stress budget of Mansour *et al.* (1988),

$$\frac{\partial R_{11}}{\partial t} = R_{11}^P + R_{11}^T + R_{11}^\Pi + R_{11}^D - R_{11}^\varepsilon + R_{11}^M,$$

where R_{11}^P, R_{11}^T, R_{11}^Π, R_{11}^D, R_{11}^ε and R_{11}^M denote the production, turbulent transport, pressure, viscous diffusion, dissipation and magnetic contributions, respectively. All terms depend solely on the separations in the homogeneous directions, r_x and r_z, and on the wall-normal coordinate y. The single-point Reynolds-stress budget reported by Mansour *et al.* (1988); Lee (2024) is recovered as the limiting case $r_x = r_z = 0$.

The corresponding spectral density $E_{11}(k_x, k_z; y)$ is obtained as the two-dimensional Fourier transform of R_{11} along the homogeneous directions, and integration over (k_x, k_z) recovers the one-point Reynolds stress. The spectra of each budget term are evaluated from the Fourier coefficients of the fluctuating velocity on the DNS grid and ensemble-averaged in time.

The spectra are visualized in the polar-logarithmic coordinates introduced by Lee & Moser (2019), in which the rescaled wavenumbers are $k_x^\# = \xi k_x/k$ and $k_z^\# = \xi k_z/k$, with $k = \sqrt{k_x^2 + k_z^2}$ and $\xi = \ln(k/k_{\text{ref}})$ for a reference wavenumber k_{ref}. Contours of constant k become arcs of constant radius ξ, the angular position encodes the orientation of a structure relative to the streamwise direction, and the rescaled spectra $E_{ij}^\# = k^2 E_{ij}/\xi$ preserve the integral identity. This representation makes the energy contained in elongated streamwise structures ($k_x^\# \to 0$) and in the diagonal isotropic tail ($k_x^\# \approx k_z^\#$) directly comparable, and is used throughout the present analysis.

RESULT

Figure 1 reports the temporal evolution of the spatially averaged centerline velocity U_c and friction velocity u_τ through the suppression and recovery transients. The two response curves are qualitatively distinct. On application of the field, U_c decreases monotonically and asymptotes smoothly towards a reduced steady value over several eddy turnover times, with no discernible overshoot. The friction velocity, $u_\tau = \sqrt{\tau_w/\rho}$, exhibits a sharp jump on switch-on, overshoots the eventual MHD steady value, and subsequently relaxes towards a level below the hydrodynamic baseline. The switch-off response is the mirror image: u_τ drops abruptly below the hydrodynamic level and recovers from below, while U_c returns smoothly over a comparable interval.

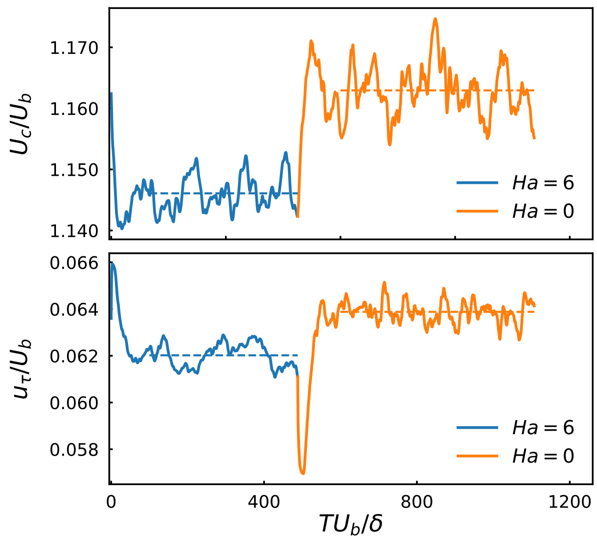

Figure 1. Temporal evolution of the spatially averaged centerline velocity U_c (top) and friction velocity u_τ (bottom), both normalized by the bulk velocity U_b, following the application and subsequent removal of the wall-normal magnetic field at $Ha = 6$.

The asymmetry between the U_c and u_τ histories reveals the separation of timescales organizing the transient. The wall-shear stress responds on the Joule timescale $\tau_J = \rho/(\sigma B^2)$, equivalent to $\mathscr{N}^{-1}$ and comparable to the eddy turnover time at $Ha = 6$. The bulk velocity, constrained by mass conservation, adjusts on the slower viscous timescale required for the mean-profile redistribution to be felt across the channel. The overshoot in u_τ is the signature of this separation: the near-wall stress responds before the mean profile has flattened. Once the mean profile has relaxed, the near-wall gradient is shallower than in the hydrodynamic case, and u_τ in the new MHD steady state lies below the hydrodynamic baseline.

This observation has two implications. First, abrupt changes in the imposed field induce rapid fluctuations in the spatially averaged wall-shear stress, an aspect of the time-dependent response that has received little quantitative attention in the wall-bounded MHD literature. Second, the asymptotic MHD state itself is unexpected. A wall-normal field is generally expected to steepen the near-wall gradient and increase the wall-shear stress (Boeck *et al.*, 2007; Krasnov *et al.*, 2008*a*; Lee, 2024), yet here τ_w lies below the hydrodynamic baseline, a direction not captured by the conventional Hartmann-layer argument. The remainder of the paper diagnoses this asymptotic state through the two-point spectral budget, both to identify the mechanism by which it is reached and to reframe the conclusion previously drawn from the integrated, one-point budget.

The origin of the skin-friction reduction is examined through the mean streamwise velocity profile and the stress balance in Figures 2 and 3. The mean-velocity profile is broadened across the bulk of the channel relative to the hydrodynamic case, with the centerline value correspondingly reduced under the constant mass-flow-rate constraint, in qualitative agreement with the three-layer structure reported for strongly magnetized Hartmann channels (Boeck *et al.*, 2007; Lee, 2024). The buffer-layer slope of $\langle U \rangle$ at $Ha = 6$ is shallower than at $Ha = 0$, and this near-wall flattening produces the reduced steady value of u_τ approached after the overshoot in Figure 1.

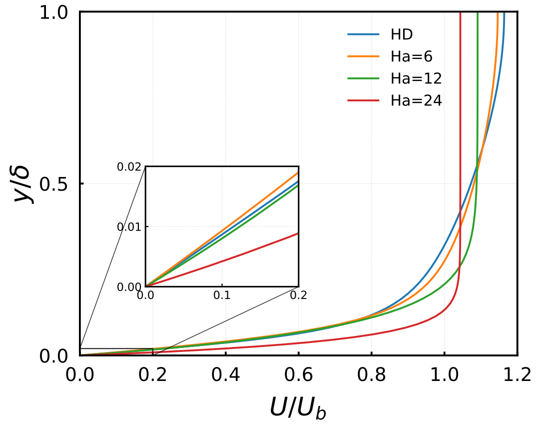

Figure 2. Mean streamwise velocity profile $\langle U \rangle/U_b$ in the hydrodynamic ($Ha = 0$) and the MHD ($Ha = 6$) statistically steady states.

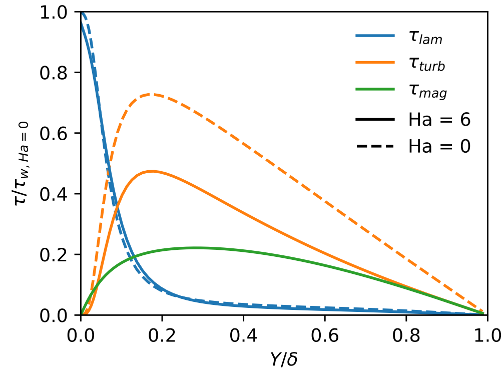

Figure 3. Laminar shear stress τ_{lam}, turbulent shear stress τ_{turb} and magnetic shear stress τ_{mag} in the asymptotic states bracketing the suppression transient, each normalized by the wall-shear stress of the hydrodynamic case.

The stress balance in Figure 3 provides a complementary view. The Lorentz force suppresses the turbulent fluctuations in the bulk and the peak of the turbulent shear stress τ_{turb} is severely blunted, while an emerging magnetic shear stress τ_{mag} takes over a substantial fraction of the total shear in the central region, in the same sense as the three-layer partition reported by Boeck *et al.* (2007) at stronger field. The wall-shear stress τ_w is governed entirely by the near-wall mean-velocity gradient. At moderate Ha, the Lorentz force attenuates the near-wall turbulent transport of momentum towards the wall, the gradient is reduced, and τ_w falls below the hydrodynamic baseline. The conventional expectation that an imposed field steepens the near-wall gradient, drawn from the Hartmann-layer solution (Hartmann, 1937; Shercliff, 1953) and the high-Ha simulations of Boeck *et al.* (2007); Krasnov *et al.* (2008*a*); Lee (2024), applies in the regime in which the thin Hartmann layer dominates. At the present $Ha = 6$, with $\mathscr{N} = Ha^2/Re$ of order 10^{-2}, the suppression of the near-wall transport outpaces the Hartmann steepening, and the net effect is a reduction in the viscous wall stress. A parametric survey across Ha would be required to delineate this regime.

This reduction in τ_w is not a reduction in pumping power. The streamwise mean momentum balance reads $|\partial_x P|\,\delta = \tau_w + \int_0^\delta |F_x|\,\mathrm{d}y$, where F_x is the streamwise Lorentz body force, so the driving pressure gradient must overcome both the wall

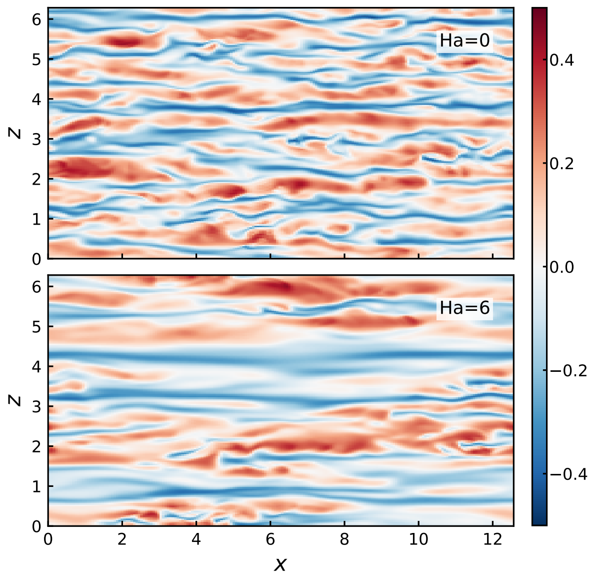

Figure 4. Instantaneous streamwise velocity fluctuation u' at $y^+ = 15$ for the hydrodynamic case ($Ha = 0$, top) and the MHD steady state ($Ha = 6$, bottom).

friction and the integrated body force. The MHD pressure drop captured by the second term is the dominant pumping cost in liquid-metal blanket flows (Smolentsev, 2021; Mistrangelo *et al.*, 2021), and the present finding is that the reduction of the near-wall turbulent transport partially offsets, but does not eliminate, this cost.

The structural counterpart of the reduced turbulent shear stress is shown in Figure 4, which reports instantaneous contours of the streamwise velocity fluctuation at $y^+ = 15$, corresponding to the peak-production location in the buffer layer. In the hydrodynamic case the flow exhibits the densely packed, meandering streaks characteristic of the near-wall cycle, whose breakdown generates the ejection and sweep events responsible for the bulk of the Reynolds shear stress (Kim *et al.*, 1987; Robinson, 1991). Under the imposed field at $Ha = 6$, the Lorentz force opposes the wall-normal and spanwise fluctuations and the near-wall streaks become highly elongated, in agreement with earlier MHD channel simulations (Lee & Choi, 2001; Boeck *et al.*, 2007; Krasnov *et al.*, 2008*a*). The flow is not fully re-laminarized: scattered patches of localized meandering remain embedded within the field, indicating that the moderate field attenuates but does not eliminate the nonlinear streak-breakdown mechanism, and the surviving bursting events constitute the source of the residual turbulent shear stress in Figure 3.

The structural modifications inferred from the instantaneous fields of the asymptotic MHD state are quantified through the two-dimensional premultiplied spectra of the budget terms, in the polar-logarithmic representation of Lee & Moser (2019). Figure 5 reports the production spectra of $\langle u'u' \rangle$, with $R_{11}^P = -\langle v'\tilde{u}' \rangle \partial_y U - \langle \tilde{v}'u' \rangle \partial_y U$, at the peak-production location in the buffer layer ($y^+ = 15$) and in the outer region ($y^+ = 90$, corresponding to one quarter of the channel height). In the buffer layer, the hydrodynamic flow exhibits a production peak at low streamwise wavenumbers and at a characteristic spanwise wavenumber, which reproduces the near-wall streak signature of canonical channel flow (Kim *et al.*, 1987; Lee & Moser, 2019). Once the field is imposed, the overall intensity of this peak is attenuated and the surviving contours become more tightly confined towards $k_x^\# \to 0$,

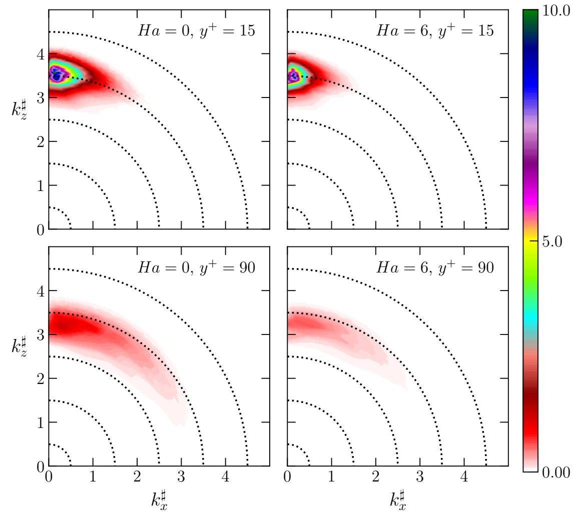

Figure 5. Two-dimensional premultiplied spectra of the production term P_{11} of $\langle u'u' \rangle$ at $y^+ = 15$ and $y^+ = 90$, for $Ha = 0$ and $Ha = 6$.

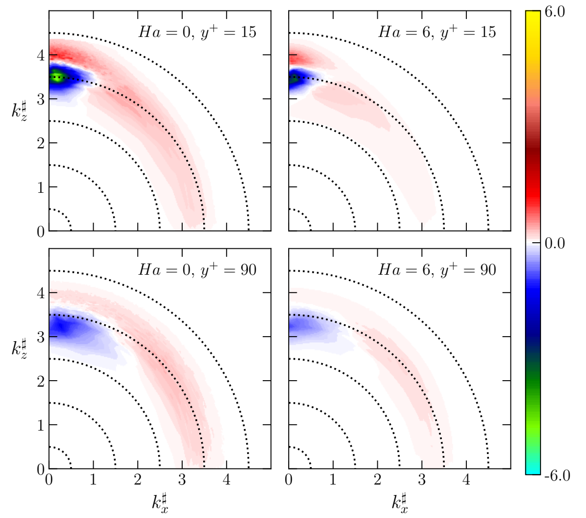

Figure 6. Two-dimensional premultiplied spectra of the turbulent interscale transfer term of $\langle u'u' \rangle$ at $y^+ = 15$ and $y^+ = 90$, for $Ha = 0$ and $Ha = 6$.

consistent with the concentration of turbulent production into elongated streamwise structures seen in Figure 4.

The same anisotropy becomes more conspicuous in the outer region. The hydrodynamic production footprint is broad and exhibits a tail extending into the range $k_x^\# \approx k_z^\#$, indicating that the energy extraction is distributed over comparatively isotropic structures, in agreement with the non-MHD results of Lee & Moser (2019); Cho *et al.* (2018). Under the imposed field, this diagonal tail is truncated. The Lorentz force operates as an anisotropic sink that selectively destroys the comparatively isotropic fluctuations, so that the surviving turbulent production is confined to highly anisotropic, streamwise-elongated scales.

Figure 6 reports the two-dimensional premultiplied spectra of R_{11}^T:

$$R_{11}^T = -\left\langle \tilde{u}'\partial_i(u_i'u') + u'\partial_i\widetilde{u_i'u'} \right\rangle + \frac{1}{2}\left\langle \partial_y(\tilde{u}'u'v') + \partial_y(u'\widetilde{u'v'}) \right\rangle$$

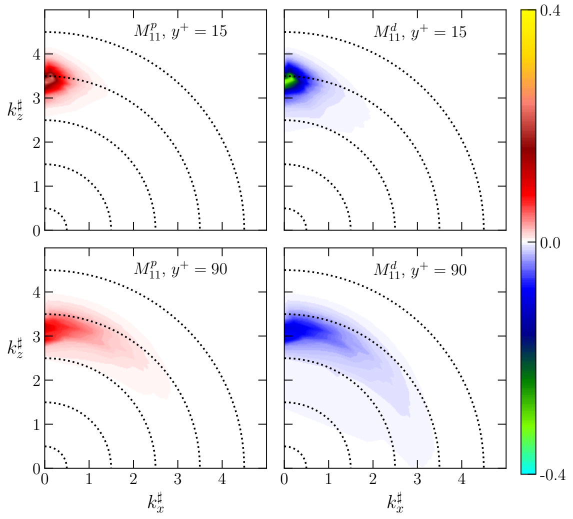

Figure 7. Two-dimensional premultiplied spectra of the magnetic potential M_{11}^p (left) and the MHD dissipation M_{11}^d (right) of $\langle u'u' \rangle$ at $Ha = 6$.

which capture how kinetic energy is exchanged between scales of different size and orientation (De Angelis *et al.*, 2002; Cimarelli *et al.*, 2016; Cho *et al.*, 2018; Kawata & Alfredsson, 2018). In the hydrodynamic case, the scale-transfer spectra display a classical forward cascade in both the buffer layer and the outer region. A concentrated negative sink coincides with the energetic large-scale streaks, and the extracted energy is deposited into the surrounding positive region, both radially outward to smaller scales and angularly into the diagonal tail at $k_x^\# \approx k_z^\#$, in agreement with the combined radial-and-angular transfer picture established for canonical wall turbulence (Lee & Moser, 2019; Cho *et al.*, 2018; Cimarelli *et al.*, 2016). The streak breakdown therefore involves both a reduction in physical size and a transition towards more isotropic, spanwise-elongated structures.

Once the field is imposed, this inter-scale and inter-directional transfer is severely choked. The intensities of the primary sink and the secondary source are markedly attenuated in the buffer layer, and the cascade into the isotropic tail is substantially weakened in the outer region. The source region remains visible along the diagonal but with reduced magnitude. The Lorentz force therefore penalizes the angular transfer of energy towards isotropic structures without entirely severing it at this moderate field strength, trapping the surviving turbulent kinetic energy within the streamwise-coherent scales and providing the spectral counterpart of the streak elongation in Figure 4. The retained fluctuation patches at $Ha = 6$ are spatially co-located across the three velocity components, the elongation of the u' streaks being accompanied by an effectively complete suppression of the v' and w' fluctuations, consistent with the anisotropy reported in earlier MHD simulations (Lee & Choi, 2001; Boeck *et al.*, 2007; Krasnov *et al.*, 2008*a*).

The effect of the electromagnetic forces on the turbulence is examined by decomposing the magnetic contribution to the streamwise Reynolds-stress budget into a magnetic potential term $R_{11}^{M_p}$ and an MHD dissipation term $R_{11}^{M_d}$, with $R_{11}^{M} = R_{11}^{M_p} + R_{11}^{M_d}$. For the present case in which the imposed field is purely wall-normal, $\mathbf{B} = (0, B_2, 0)$ with $|B_2| = 1$, and the two contributions reduce to $R_{11}^{M_p} = \mathcal{N} \left\langle \tilde{u}' \partial_z \phi' + u' \partial_z \tilde{\phi}' \right\rangle$, and $R_{11}^{M_d} = -2\mathcal{N} \left\langle \tilde{u}' u' \right\rangle$. Figure 7 presents the two-dimensional premultiplied spectra of M_{11}^p and M_{11}^d, both of which vanish identically in the hydrodynamic case.

Once the magnetic field is imposed, the magnetic potential term emerges as a highly localized source of kinetic energy. In the buffer layer, this source is strictly confined to the largest streamwise scales ($k_x^\# \to 0$) and to the characteristic spanwise streak spacing ($k_z^\# \approx 3.5$), and acts to inject a fraction of the electromagnetic work into the primary streamwise streaks. In the outer region, the same injection follows the anisotropic filtering established in the preceding sections and feeds predominantly the elongated, streamwise-coherent structures rather than the broader diagonal tail.

The MHD dissipation term, by contrast, operates as a strong energy sink. Its spectral footprint is found to be nearly a mirror image of the magnetic potential source, with the bulk of its intensity localized at the same scales ($k_x^\# \to 0$) across the channel. The Lorentz force is therefore not a uniform broadband damper of the fluctuating motion, and acts instead selectively on the most energetic, streamwise-coherent structures of the flow.

The sum $M_{11}^p + M_{11}^d$ is found to cancel almost exactly over the bulk of the spectral plane, so that two individually large contributions leave only a modest residual once summed. The residual, however, is not uniformly distributed. Its negative lobe is concentrated in the low-$k_x^\#$ range at the characteristic spanwise streak spacing, indicating that the net magnetic work is dissipative and scale-localized on the most energetic, streamwise-coherent structures rather than on the comparatively isotropic fluctuations at larger $k_x^\#$. The spectral decomposition therefore reframes the conclusion drawn from the integrated, one-point budget reported in Yamamoto & Kunugi (2016); Lee (2024), in which the magnetic contribution to $\langle u'^2 \rangle$ was found to be small. The present results indicate that the small integrated value is the residual of two much larger spectral contributions that cancel nearly completely, and that the Lorentz force is in fact far from negligible: it acts strongly and selectively on a narrow band of streamwise-coherent scales and bleeds kinetic energy out of the primary streaks at a rate that is invisible to the one-point budget.

CONCLUSIONS

The transient response of incompressible turbulent channel flow at $Re_\tau = 182$ to the sudden application and removal of a wall-normal magnetic field at $Ha = 6$ has been investigated through direct numerical simulation, and the asymptotic MHD state has been characterized through the two-point spectral budget of the streamwise Reynolds stress in the polar-logarithmic representation of Lee & Moser (2019). The friction velocity is found to overshoot its eventual MHD value on switch-on and to undershoot the hydrodynamic baseline on switch-off, in contrast with the smooth, monotonic adjustment of the centerline velocity, and this asymmetry reflects the separation between the rapid Joule timescale on which the wall-shear stress responds and the slower viscous timescale that governs the redistribution of the mean profile. The new MHD steady state is found to exhibit a wall-shear stress that lies below the hydrodynamic baseline, in a direction not anticipated by the conventional Hartmann-layer argument, because at this moderate interaction parameter the suppression of the near-wall turbulent transport outpaces the steepening of the mean-velocity gradient, although this reduction in τ_w does not translate into a reduction of the pumping power once the integrated Lorentz body force is accounted for in the streamwise momentum balance. The two-point spectral budget reveals that the Lorentz force selectively attenuates the diagonal $k_x^\# \approx k_z^\#$ branch of the production and the inter-scale transfer, so that the surviving turbulent kinetic energy is trapped within streamwise-coherent scales, in quantitative agreement with the streak elongation observed in the instantaneous fields. The decomposition of the magnetic contribution into a magnetic potential source M_{11}^p and an MHD dissipation sink M_{11}^d shows that the two terms are individually large and cancel almost exactly over most of the spectral plane, leaving a residual net sink concentrated in the low-$k_x^\#$ range at the characteristic spanwise streak spacing, so that the small net magnetic contribution previously reported in the integrated, one-point budget of Yamamoto & Kunugi (2016); Lee (2024) is reframed as the residual of a strongly scale-localized exchange that bleeds kinetic energy out of the surviving streamwise-coherent streaks at moderate Ha and that bears directly on the transient electromagnetic loading encountered in molten-salt blanket flows.

ACKNOWLEDGEMENT

An award of computer time was provided by the Innovative and Novel Computational Impact on Theory and Experiment (INCITE) program. This research used resources of the Argonne Leadership Computing Facility, which is a DOE Office of Science User Facility supported under Contract DE-AC02-06CH11357.

REFERENCES

Abdou, M., Morley, N. B., Smolentsev, S., Ying, A., Malang, S., Rowcliffe, A. & Ulrickson, M. 2015 Blanket/first wall challenges and required R&D on the pathway to DEMO. *Fusion Engineering and Design* **100**, 2–43.

Al-Habahbeh, O M, Al-Saqqa, M, Safi, M & Khater, T Abo 2016 Review of magnetohydrodynamic pump applications. *Alexandria Engineering Journal* **55**, 1347–1358.

Boeck, Thomas, Krasnov, Dmitry & Zienicke, Egbert 2007 Numerical study of turbulent magnetohydrodynamic channel flow. *Journal of Fluid Mechanics* **572**, 179–188.

Cho, M., Hwang, Y. & Choi, H. 2018 Scale interactions and spectral energy transfer in turbulent channel flow. *Journal of Fluid Mechanics* **854**, 474–504.

Cimarelli, A., De Angelis, E., Jiménez, J. & Casciola, C. M. 2016 Cascades and wall-normal fluxes in turbulent channel flows. *Journal of Fluid Mechanics* **796**, 417–436.

Davidson, P. A. 2017 *Introduction to Magnetohydrodynamics*, 2nd edn. Cambridge University Press.

De Angelis, E., Casciola, C. M. & Piva, R. 2002 The scale-by-scale kinetic energy budget near the turbulent/non-turbulent interface. *Computers & Fluids* **32**, 495–507.

Hartmann, J. 1937 Hg-Dynamics I. Theory of the Laminar Flow of an Electrically Conductive Liquid in a Homogeneous Magnetic Field. *Mathematisk-fysiske Meddelelser. XV, 6* .

Jiang, Yuchen & Smolentsev, Sergey 2024 Characterization of the MHD flow and pressure drop in the access ducts of a liquid metal fusion blanket. *Fusion Engineering and Design* **201**, 114262.

Kawata, T. & Alfredsson, P. H. 2018 Inverse interscale transport of the Reynolds shear stress in plane Couette turbulence. *Physical Review Letters* **120**, 244501.

Kim, J., Moin, P. & Moser, R. 1987 Turbulence statistics in fully developed channel flow at low reynolds number. *Journal of Fluid Mechanics* **177**, 133–166.

Krasnov, Dmitry, Zikanov, Oleg & Boeck, Thomas 2012 Numerical study of magnetohydrodynamic duct flow at high Reynolds and Hartmann numbers. *Journal of Fluid Mechanics* **704**.

Krasnov, Dmitry, Zikanov, Oleg, Schumacher, Jörg & Boeck, Thomas 2008*a* Magnetohydrodynamic turbulence in a channel with spanwise magnetic field. *Physics of Fluids* **20**.

Krasnov, D., Zikanov, O., Schumacher, J. & Boeck, T. 2008*b* Magnetohydrodynamic turbulence in a channel with spanwise magnetic field. *Physics of Fluids* **20**, 095105.

Lee, D. & Choi, H. 2001 Magnetohydrodynamic turbulent flow in a channel at low magnetic reynolds number. *Journal of Fluid Mechanics* **439**, 367–394.

Lee, Myoungkyu 2024 Direct Numerical Simulation of Magnetohydrodynamic Turbulent Channel Flows. In *Proceeding of Thirteenth International Symposium on Turbulence and Shear Flow Phenomena*.

Lee, M. & Moser, R. 2015 Direct numerical simulation of turbulent channel flow up to $Re_\tau = 5200$. *Journal of Fluid Mechanics* **774**, 395–415.

Lee, M. & Moser, R. 2019 Spectral analysis of the budget equation in turbulent channel flows at high reynolds number. *Journal of Fluid Mechanics* **860**, 886–938.

Mansour, N. N., Kim, J. & Moin, P. 1988 Reynolds-stress and dissipation-rate budgets in a turbulent channel flow. *Journal of Fluid Mechanics* **194**, 15–44.

Mistrangelo, C., Bühler, L., Smolentsev, S., Klüber, V., Maione, I. & Aubert, J. 2021 MHD flow in liquid metal blankets: Major design issues, MHD guidelines and numerical analysis. *Fusion Engineering and Design* **173**.

Mizuno, Y. 2016 Spectra of energy transport in turbulent channel flows for moderate Reynolds numbers. *Journal of Fluid Mechanics* **805**, 171–187.

Pothérat, A. & Kornet, K. 2015 The decay of wall-bounded MHD turbulence at low *Rm*. *Journal of Fluid Mechanics* **783**, 605–636.

Robinson, S. K. 1991 Coherent motions in the turbulent boundary layer. *Annual Review of Fluid Mechanics* **23**, 601–639.

Satake, S., Kunugi, T., Takase, K. & Ose, Y. 2006 Direct numerical simulation of turbulent channel flow under a uniform magnetic field for large-scale structures at high reynolds number. *Physics of Fluids* **18**, 125106.

Shercliff, J. A. 1953 Steady motion of conducting fluids in pipes under transverse magnetic fields. *Mathematical Proceedings of the Cambridge Philosophical Society* **49**, 136–144.

Smolentsev, S. 2021 Physical background, computations and practical issues of the magnetohydrodynamic pressure drop in a fusion liquid metal blanket. *Fluids* **6**, 110.

Yamamoto, Yoshinobu & Kunugi, Tomoaki 2016 MHD effects on turbulent dissipation process in channel flows with an imposed wall-normal magnetic field. *Fusion Engineering and Design* **109**, 1137–1142.

Zikanov, O., Krasnov, D., Boeck, T., Thess, A. & Rossi, M. 2014 Laminar-turbulent transition in magnetohydrodynamic duct, pipe, and channel flows. *Applied Mechanics Reviews* **66**, 030802.

Zikanov, O. & Thess, A. 1998 Direct numerical simulation of forced mhd turbulence at low magnetic reynolds number. *Journal of Fluid Mechanics* **358**, 299–333.